ACS OMEGA

Open Access

http://pubs.acs.org/journal/acsodf

Article

Ru-Doped MoS_2 Monolayer for Exhaled Breath Detection on Early Lung Cancer Diagnosis: A First-Principles Investigation

Xiaoqi Chen and Qianqian Wan*

Cite This: *ACS Omega* 2024, 9, 13951−13959

Read Online

ACCESS | Metrics & More | Article Recommendations

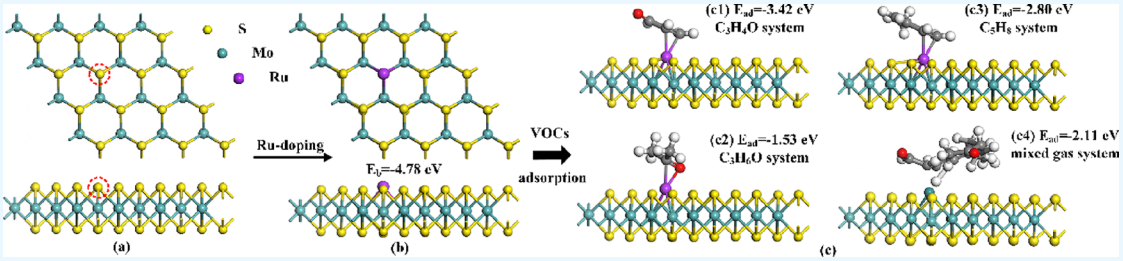

ABSTRACT: Nanosensor-based patient exhaled breath detection is a practical and effective way to detect lung cancer early. In this paper, a Ru-doped MoS_2 monolayer (Ru-MoS_2) is proposed as a promising novel biosensor based on first-principles theory for the detection of three typical early stage lung cancer exhaled volatile organic compounds, namely, C_3H_4O, C_3H_6O, and C_5H_8. Replacement of a S atom in the MoS_2 monolayer with a Ru dopant atom to form a stable Ru-MoS_2 monolayer with a binding energy of −4.78 eV is further demonstrated by the thermostability and chemical stability analysis as well as improving the adsorption performance of the system for three VOCs. The adsorption configuration structures, adsorption properties, and electronic behavior of the Ru-MoS_2 monolayer are investigated by electron deformation density and density of states analysis to gain a comprehensive understanding of the physicochemical properties as sensing material. The results show that the adsorption energies of the Ru-MoS_2 monolayer for C_3H_4O, C_3H_6O, and C_5H_8 are 3.42, −1.53, and −2.80 eV, respectively, all of which are chemisorption with excellent adsorption performance. The sensitivities for the three VOCs could be up to 1.09, 140.50, and 5.90, respectively, and the band structure and work function further elucidate the sensing mechanism of the Ru-MoS_2 monolayer as a resistive gas sensor. The type and concentration of these exhaled breaths may reflect changes in the patient's physiological and biochemical status and may serve as a probe for the diagnosis of lung cancer. The results in this work could provide a guidance for researchers to explore the practical applications in the early diagnosis of lung cancer by gas sensors.

1. INTRODUCTION

Lung cancer is the second leading cause of death worldwide after heart disease, killing 1.6 million people each year. Histologically, lung cancer is divided into nonsmall cell lung cancer (NSCLC), which accounts for about 85% of cases, and small cell lung cancer (SCLC), which accounts for the remaining 15%. A total of 85% of lung cancer cases are diagnosed at an advanced stage, and the 5 year survival rate is only about 10−15%.[1−3] However, if the disease is diagnosed at stage 1, the 5 year survival rate increases dramatically to 80%. The presence and staging of disease can be confirmed using current diagnostic techniques such as blood tests, chest X-rays, computed tomography (CT), magnetic resonance imaging (MRI), and positron emission tomography (PET).[4−6] Genetic analysis and protein analysis are novel technologies for determining cancer risk, prognosis, and targeted (or individualized) therapy. Despite the progress made in recent years in identifying biomarkers, mutations, and genomic signatures, there are still formidable hurdles to overcome on developing effective biomarkers, such as tumor heterogeneity, highly complex tumor−host interactions, and the complexity, diversity, and redundancy of tumor−cell signaling networks involving genetic, epigenetic, and microenvironmental effects. Furthermore, the technologies associated with these methods are often expensive, time-consuming, and unavailable in many healthcare settings and require relatively large amounts of tissue for analysis.[7,8] Thus, the search for diagnostic methods for early lung cancer detection is critical and urgent.

In recent years, an emerging approach through the detection of volatile organic compounds (VOCs), which can be detected in the headspace of cancer cells or blood samples or in exhaled

Received: November 18, 2023
Revised: February 22, 2024
Accepted: February 29, 2024
Published: March 15, 2024

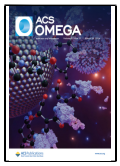

https://doi.org/10.1021/acsomega.3c09191
ACS Omega 2024, 9, 13951−13959

breath, has come to the attention of researchers.[9−11] On account of the simplicity, efficiency, and low cost of the method, monitoring VOCs in breath may soon become a promising approach to traditional medical diagnostics. Tumors growing in the body have been reported to produce specific substances that release VOCs into the bloodstream and exchange with them in the lungs. Moreover, lung cancer patients have significantly higher levels of VOCs in their exhaled breath than healthy individuals, which offers the possibility of identifying possible lung cancer patients and assessing the severity of the diagnosed patients. Gordon et al.[12] selected a total of 22 kinds of VOCs that are considered to be characteristic levels in the exhaled breath of lung cancer patients, mainly alkanes and benzene derivatives. Among them, 2-acrylaldehyde diol (C_3H_4O), acetone (C_3H_6O), and isoprene (C_5H_8) are typical biomarkers that can show the severity of lung dysfunction in humans. Exhaled breath analysis tests for lung cancer using nanomaterial-based sensor arrays were reportedly proposed by Barash et al.[13] Chang and his colleagues[3] used the sensor system to analyze VOCs in exhaled breath for lung cancer diagnosis. Thus, the detection of specific VOCs in exhaled breath by highly sensitive and fast-responding chemical sensors could provide a simple, painless, and non-invasive test for early lung cancer diagnosis, which could be a promising diagnostic modality.

Due to its extraordinary physical, chemical, optical, and mechanical qualities, the MoS_2 monolayer, one of the transition metal dichalcogenides (TMDs), has attracted a lot of attention for applications in gas sensors lately.[14,15] Three atomic layers of S−Mo−S make up the MoS_2 monolayer, where the Mo atom is covalently bound to six S atoms to form a sandwiched substance, with a band gap of 1.9 eV.[16−19] However, the MoS_2 monolayer is chemically inert due to the absence of defects. Over the past few years, it has been demonstrated that the chemical activity and sensitivity of MoS_2 monolayer substrates can be greatly improved by introducing defects and appropriate metal dopants.[20−22] The characteristics of 2D materials, such as their increased sensitivity to tiny molecules and increased chemical activity, can be changed by incorporating the right transition metal elements. Zhao et al.[23] concluded that the Cu-embedded MoS_2 monolayer worked the best after a thorough analysis of the effects of doping MoS_2 for oxygen reduction reaction with 19 different types of transition elements. Fan et al.[24] conducted a theoretical investigation into the adsorption of CO, NO, O_2, NO_2, and NH_3 on 10 TM-doped MoS_2 surfaces. The results showed that the chemical activity and adsorption performance of gas molecules on the doped MoS_2 surfaces were significantly improved at 3.12 eV adsorption energies as compared to those of the intrinsic MoS_2 monolayer. Therefore, the influence of suitable transition metal dopants on the chemical and catalytic properties of the MoS_2 monolayer is crucial, which may have great potential for VOC sensing.

To explore gas sensing materials with high sensitivity to VOCs and then promote the development of cutting-edge sensors for the diagnosis of early lung cancer, the density functional theory-based theoretical calculations regarding the adsorption performance of Ru-doped MoS_2 (Ru-MoS_2) toward three typical VOCs (C_3H_4O, C_3H_6O, and C_5H_8) associated with lung cancer have been conducted in this work, and the feasibility of the Ru-MoS_2 monolayer as resistive gas sensing material for VOC detection has been discussed theoretically. The Ru-MoS_2 structure is produced by substituting a S atom from the MoS_2 monolayer for the Ru atom, which has demonstrated excellent catalytic performance for gas interactions. To thoroughly examine its property as a chemical sensor, the adsorption configuration structures, adsorption properties, electronic behavior, and the sensing mechanism of the Ru-MoS_2 monolayer are further investigated. Our findings demonstrate that the doping of Ru could greatly enhance the adsorption performance of MoS_2 on VOCs and the potential of the Ru-MoS_2 monolayer as a viable sensor for VOC detection, opening up to further research into its application in the diagnosis of lung cancer. Our calculations provide a theoretical basis for future practical applications of gas biosensors in the field of lung cancer prognosis.

2. COMPUTATIONAL DETAILS

The density functional theory method was used to implement the entire calculation in the Dmol^3 program. To handle electron exchange and correlation, the Perdew−Burke−Ernzerhof (PBE) function with generalized gradient approximation (GGA) was used.[25,26] To address the relativistic effect of the Ru atom, we selected the DFT semicore pseudopotential (DSSP) approach and double numerical plus polarization (DNP) as the atomic orbital basis set. The Tkatchenko and Scheffler (TS) approach was used to gain a deeper comprehension of the van der Waals interaction.[27,28] For geometric optimization and electronic structure computations, the Monkhorst−Pack k-point mesh of $10 \times 10 \times 1$ was taken for the Brillouin zone integration. We decided on 10^{-4} Ha for the energy tolerance accuracy, 2×10^{-2} Ha/Å for the maximum force, and 5×10^{-2} Å for the displacement.[29,30] To provide correct findings for total energy estimates in static electronic structure calculations, a 10^{-6} Ha self-consistent loop energy, a global orbital cutoff radius of 5.0 Å, and a smearing of 0.005 Ha were used. Each and every calculation was spin-polarized.[31]

A $4 \times 4 \times 1$ MoS_2 monolayer supercell with a 20 Å vacuum area is created that contains 16 Mo and 32 S atoms. For additional adsorptions, it is then loosened to its most stable state. The optimized lattice parameter of the MoS_2 monolayer was calculated as 3.18 Å, which is fairly close to the previous report. The following formula is used to determine each gas adsorption process's adsorption energy (E_{ad}).

$$E_{ad} = E_{Ru-MoS_2/gas} - E_{Ru-MoS_2} - E_{gas} \quad (1)$$

wherein $E_{Ru\text{-}MoS_2/gas}$, $E_{Ru\text{-}MoS_2}$, and E_{gas} were the energies of the Ru-MoS_2 surface after gas molecule adsorption, isolated Ru-MoS_2, and the individual gas molecule, respectively. An exothermic, spontaneous adsorption occurs if $E_{ad} < 0$; the more dramatic the adsorption behavior, the larger the absolute value. Alternatively, the interaction cannot occur if E_{ad} is less than 0. The charge transfer (Q_T) between the target molecule and the adsorbent surface, which is defined by the electron value carried by the gas molecule following adsorption, was examined by using the Hirshfeld method. The converge criterion and cutoff parameter mentioned above have been used to optimize the various structures. The initial distances between the gas molecules and the transition metal are all set at 2.0 Å.

3. RESULTS AND DISCUSSION

3.1. Analysis of the Ru-MoS_2 Monolayer and Gas Molecules. Three distinct exhaled volatile organic compounds

https://doi.org/10.1021/acsomega.3c09191
ACS Omega 2024, 9, 13951−13959

(VOCs) of lung cancer patients are plotted in Figure 1. Calculations reveal that the bond lengths and bond angles of

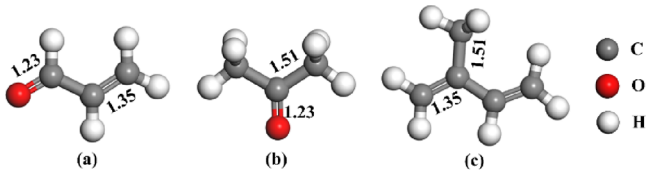

Figure 1. Geometric structure of (a) C_3H_4O, (b) C_3H_6O, and (c) C_5H_8.

these gas molecules are almost identical to those reported previously,[32] which further illustrates the validity of VOC models. Therefore, a detailed analysis is not given here.

The electron deformation density (EDD) of the Ru-MoS_2 monolayer and the most stable model of the MoS_2 monolayer before and after Ru atom doping are depicted in Figure 2. Since monosulfur vacancies are the most prevalent point defect structure and have a lower formation energy than Mo vacancies, the Ru atom is selected to replace the S atoms in MoS_2 to generate the Ru-MoS_2 monolayer. Ru doping causes the MoS_2 monolayer to undergo certain notable deformations. Upon measurement, Ru is measured to form Ru−Mo bonds with three neighboring Mo atoms with the bond length of 2.647 Å, which is slightly longer than the original Ru−Mo bond on account of the larger atomic radii of the Ru atom in comparison to the S atom. The binding force (E_b) is determined to be −4.78 eV with Ru doping on the MoS_2 surface, indicating a significant contact between the Ru dopant and the MoS_2 monolayer.

The Hirshfeld method indicates that the Ru dopant contributes 0.097 e to the MoS_2 surface during doping, referring to its electron-donating property on the MoS_2 surface. The surrounding Mo atoms are surrounded by electron accumulation, whereas the Ru atom is surrounded by electron depletion, as can be seen from the EDD distribution. The ionic character of the Ru−Mo bonds and their strong orbital interaction during Ru doping are confirmed by the obvious electron overlaps on them. Moreover, with the goal of determining if the Ru-MoS_2 monolayer can be stabilized at 500 K and considering the potential for their development for gas-sensitive medical devices, the thermostability is confirmed using molecular dynamic simulation for 1 ps, with a step of 1 fs. It can be found that the morphology of the Ru-MoS_2 monolayer is in a stable configuration after 1000 stem simulations at 500 K. Consequently, it is concluded that the Ru-MoS_2 monolayer exhibits high thermostability. Additionally, the vibrational analysis reveals that the Ru-MoS_2 monolayer has frequencies that range from 59.8 to 455.2 cm^{-1}, indicating high chemical stability in the absence of an imaginary frequency.

To further comprehend the electron property of Ru doping onto the pure MoS_2 monolayer, Figure 3 plots the density of state (DOS) of the Ru-MoS_2 system in comparison to pristine MoS_2 and the orbital DOS of the Ru and S atoms. As compared to pure MoS_2, the result demonstrates a considerable leftward shift in the DOS curves of Ru-MoS_2, especially near the Fermi energy level, where it exhibits a new peak known as the impurity state, which can be attributed to the contribution of Ru doping and its hybridization states with S and Mo atoms. In addition, the new state introduced by the Ru dopant improves the chemical reactivity and electronic activity of the Ru-MoS_2 monolayer to some extent. Strong orbital interactions between Ru and Mo atoms in Figure 3b are implied by the observation that the Ru 4d orbital is highly hybridized with the Mo 4d orbital from −6.25 to 2.0 eV and −12.0 to −13.2 eV, which is consistent with the EDD distribution in which the Ru−Mo bond is surrounded by electron accumulation.

3.2. Gas Adsorption Configurations on the Ru-MoS_2 Monolayer. Adsorptions of C_3H_4O, C_3H_6O, and C_5H_8 are carried out on the surface of the Ru-MoS_2 monolayer with its optimal structure. Various adsorption configurations are implemented with an optimum initial adsorption distance of 2.0 Å to obtain the most stable configuration. The geometric structures and associated EDD for the three VOC systems are shown in Figure 4.

When C_3H_4O is adsorbed on the Ru-MoS_2 surface at an angle, it is seen that the C_3H_4O molecule prefers to stand vertically on top of the Ru dopant on a slope, trapped by the Ru atom to form two new Ru−C bonds with measured diameters of 2.211 and 2.146 Å. This result implies that the binding force between Ru and C atoms is greater than the binding force between Ru and O atoms. Following C_3H_4O adsorption, the Ru−Mo bond exhibits a substantial deformation, suggesting that the Ru-MoS_2 monolayer is geometrically activated during gas interaction. The E_{ad} of −3.42 eV in this system is categorized as chemisorption. However, this chemisorption is much stronger than that in the pristine MoS_2 system, in which an E_{ad} of −1.57 eV is obtained as calculated, indicating that Ru doping effectively enhances the adsorption performance of the MoS_2 monolayer on C_3H_4O. Apart from that, compared with the previous report, the Ru-MoS_2 monolayer in this study shows higher adsorption energy

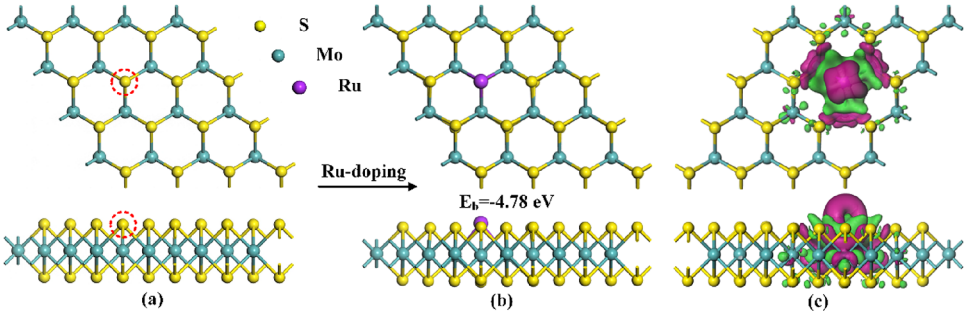

Figure 2. Ru doping process on the MoS_2 monolayer. Morphology of (a) the intrinsic MoS_2 monolayer, (b) Ru-MoS_2 monolayer, and (c) EDD of Ru-MoS_2 monolayer. In EDD, the green (rosy) areas indicate electron accumulation (depletion) and the isosurface is set as 0.01 eV/A^3.

https://doi.org/10.1021/acsomega.3c09191
ACS Omega 2024, 9, 13951−13959

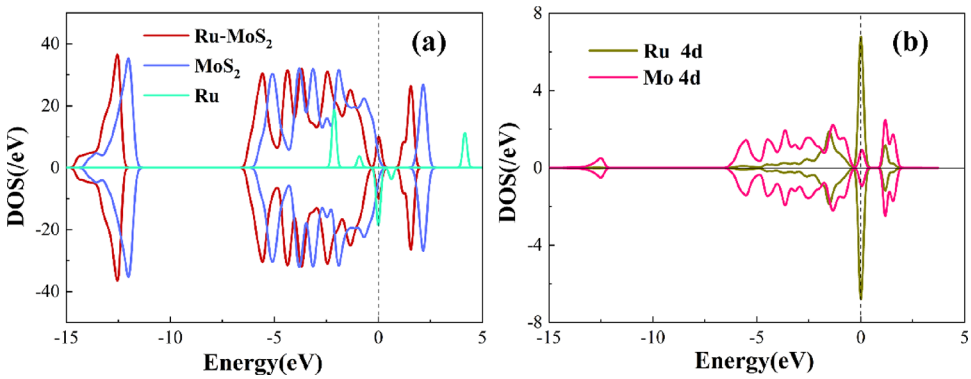

Figure 3. (a) DOS comparison before and after doping Ru and (b) orbital DOS in the Ru-MoS_2 system. The dashed line in DOS is the Fermi level.

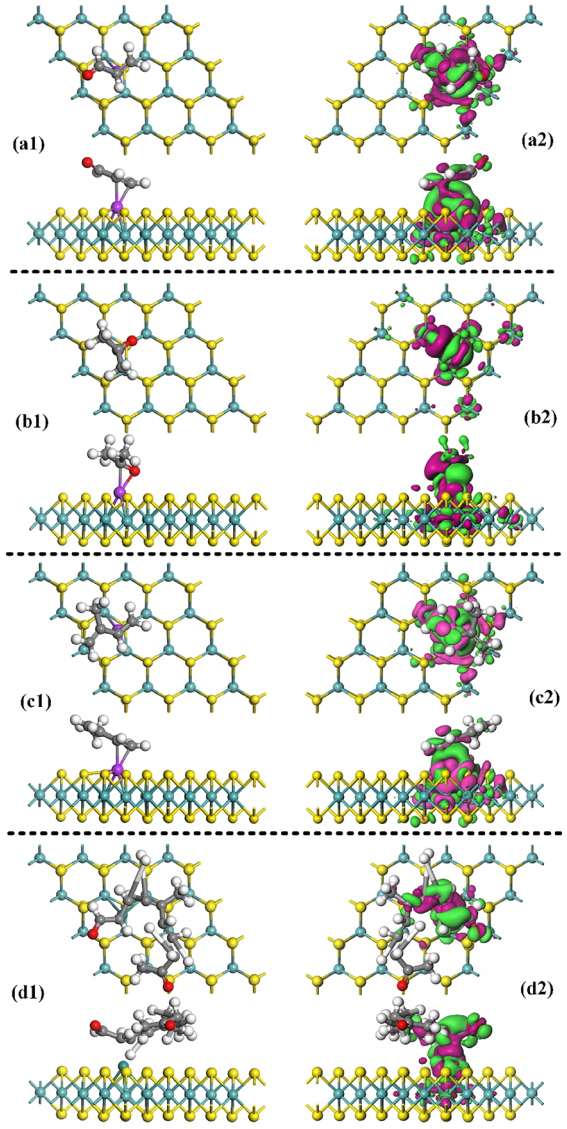

Figure 4. Optimized structure and EDD of the C_3H_4O system (a1, a2), C_3H_6O system (b1, b2), C_5H_8 system (c1, c2), and mixed gas adsorption system (d1, d2). In EDD, the green (rosy) areas indicate electron accumulation (depletion).

for C_3H_4O than Ni-doped MoS_2 (−1.749 eV), indicating the superiority of Ru element doping.[17] The Hirshfeld study also shows that the Ru atom is assigned a positive charge of 0.130 e, and the C_3H_4O molecule as a whole has a negative charge of 0.225 e. These findings suggest that the Ru dopant (0.130 e) and Ru-MoS_2 monolayer (0.095 e) are responsible for 0.225 e that C_3H_4O accepts, which indicates that the Ru-MoS_2 surface is electron-donating, while the C_3H_4O molecule is electron-absorbing. The Ru dopant is surrounded by electron depletion in the EDD distribution, whereas the Ru−C and Ru−O bonds are surrounded by electron accumulation, which confirms the electron-releasing behavior of the Ru atoms and the electron hybridization on the newly formed bonds.

It is discovered that following C_3H_6O adsorption onto the Ru-MoS_2 monolayer, the C_3H_6O molecule is parallel to the Ru-MoS_2 surface and exhibits minimal geometric distortion, which is not as drastic as those in the C_3H_4O system, suggesting that the interactions in the C_3H_6O system are weaker. The Ru dopant captures a C atom and an O atom from the C_3H_6O molecule, forming new Ru−C and Ru−O bonds that measure 2.179 and 2.015 Å, respectively. Furthermore, the computed E_{ad} in this instance is −1.53 eV, which is less than that of C_3H_4O, indicating chemisorption. Nevertheless, as a result of Ru doping, the adsorption performance of the Ru-MoS_2 monolayer on C_3H_6O is noticeably improved compared to that of pristine MoS_2 (−0.20 eV), which indicates that the Ru dopant boosts the redistribution of the electrons and provides more adsorption sites. As can be seen from EDD, the adsorbed C_3H_6O molecule has a negative charge of 0.133 e, showing a relatively weak electron gain. Electron depletion is mainly concentrated on the keto group, while electron accumulation occurs mainly on the Ru−O and Ru−C bonds, which confirms the strong bonding between the Ru dopant and the O and C atoms.

In terms of the C_5H_8 adsorption system, the optimized configuration is comparable to that of the C_3H_4O system, wherein the two C atoms in the C═C bond form new bonds with the Ru dopant with bond lengths of 2.145 and 2.212 Å, respectively, and the C_5H_8 molecule is tilted in the Ru-MoS_2 plane. These results imply that the Ru dopant is highly chemically reactive to the C═C bond. The E_{ad} of this system is −2.80 eV, second only to that of the C_3H_4O system, and its adsorption efficiency surpasses that of the MoS_2 system (−1.36 eV). Furthermore, the adsorption energy is still larger than that of the previously reported Al-$MoSe_2$ monolayer toward C_5H_8 (−2.00 eV), which exhibits excellent adsorption properties of the Ru-MoS_2 monolayer.[25] According to the Hirshfeld analysis, the C_5H_8 molecule obtained a transfer of 0.120 e from the Ru-MoS_2 surface, while the Ru atom loses 0.11 e during this adsorption process. As can be seen from EDD, the charge source is mainly from the Ru atom of the Ru-MoS_2 monolayer,

https://doi.org/10.1021/acsomega.3c09191
ACS Omega 2024, 9, 13951−13959

which is transferred to the C_5H_8 molecule mainly through two Ru−C bonds. These results clarify the charge-transfer mechanism, the synthesis of the chemical Ru−C bonds, and the localization of charge.

Apart from this, the simultaneous adsorption of the three VOCs on the Ru-MoS_2 surface is further explored. As can be seen from Figure 4d1, after the three gases are adsorbed, the shape of the gas molecules undergoes obvious deformation and some of the chemical bonds are elongated, indicating that a strong adsorption reaction is generated. The calculations show that the adsorption energy of the Ru-MoS_2 monolayer for the three gas mixtures is −2.11 eV, and the Ru atom behaves as an electron contributor, losing 0.0819 e. Since the charge transfer of the adsorption process of the Ru-MoS_2 monolayer for a single gas is in the same direction, the adsorption of the Ru-MoS_2 monolayer for the gas mixtures is synergistic. Figure 4d2 demonstrates EDD for the adsorption of mixed gases by the Ru-MoS_2 monolayer, from which the direction of charge transfer can be clearly seen. It can be found that a large amount of charge transfer mainly occurs near the Ru atom, indicating that the doping of the Ru atom promotes electron redistribution and increases the adsorption sites of gases.

In summary, the adsorption of the Ru-MoS_2 monolayer on the three VOCs is chemisorption, and the adsorption capacity is ranked as C_3H_4O > C_5H_8 > C_3H_6O. Compared with other studies on the adsorption of VOCs by gas sensing materials (Table 1), the Ru-MoS_2 monolayer proposed in this study has

Table 1. Adsorption Performance of Various Gas Sensors toward VOCs

gas sensing material	target gas	E_{ad} (eV)
Ni-MoS_2[17]	C_5H_8	−1.84
	C_3H_4O	−1.75
	C_6H_6	−1.52
Al-$MoSe_2$[25]	C_3H_4O	−1.45
	C_3H_6O	−1.80
	C_5H_8	−2.00
Ru-$PtTe_2$[32]	C_3H_4O	−1.72
	C_3H_6O	−1.12
	C_5H_8	−1.80
Au-SnS_2[26]	C_3H_6O	−0.77
	C_5H_8	−1.31
	C_6H_6	−0.71
Pt-SnS[27]	C_2H_4	−0.53
	C_2H_6	−0.31
	C_6H_6	−0.60
Ru-MoS_2 in this work	C_3H_4O	−3.42
	C_3H_6O	−1.53
	C_5H_8	−2.80

significant advantages in adsorption performance. Meanwhile, the doping of the Ru atom promotes the charge transfer-induced electron redistribution, which dramatically improves the adsorption performance of the MoS_2 monolayer on the three gases.

3.3. Electronic Property of the Ru-MoS_2 Monolayer upon Gas Adsorption. For the purpose of understanding the electronic behavior of the Ru-MoS_2 monolayer following gas adsorption, the DOS distributions of various VOC systems are shown in Figure 5. The findings demonstrated that there are varying degrees of change in the overall DOS distributions of the Ru-MoS_2 monolayer-adsorbed target molecules. The electronic behavior is evident in the total DOS distribution for the C_3H_4O molecular adsorption system, as depicted in Figure 5a1. It can be noticed that the peaks at the Fermi energy level become weaker, while several new peaks appear near −11.2, −8.9, and 1.8 eV compared to the total DOS of the Ru-MoS_2 monolayer alone. It is hypothesized that these deformations are caused by the interaction between Ru 4d and C 2p. The DOS peak of Ru 4d in the C_3H_4O system is noticeably less than the partial DOS in the Ru-MoS_2 system in Figure 3, which can further support the above findings. Furthermore, following the adsorption of C_3H_4O, a change in DOS is caused by the strong hybridization of Ru 4d with C 2p between −8.9 and 1.8 eV. The electronic behavior of the C_5H_8 adsorption system, as depicted in Figure 5c1, is comparable to that of the C_3H_4O system. However, fewer splitting peaks and recombination peaks of the total DOS are produced, further demonstrating a marginally weaker chemical interaction between the C_5H_8 molecule and the adsorbent surface. In the C_3H_6O system, the overall DOS curve after adsorption of the target gas is shifted to the right, which is attributed to the electron-contributing property of the Ru-MoS_2 surface. During the gas adsorption process, electrons are transferred from the Ru-MoS_2 surface to the gas molecule, which reduces the carrier density of the surface and thus reduces the conductivity of Ru-MoS_2. In addition, the highly activated C 2p and O 2p orbitals of C_3H_6O are responsible for the notable enhancement of the Fermi energy level peaks and the new states at −8.3 and −6.5 eV, which show a major shift in its electronic behavior. Moreover, the overlapping region in the partial DOS at −6.8 to 2.0 eV suggests certain orbital hybridizations between the C and O atoms of the C_3H_6O molecule and Ru-MoS_2 monolayer. Figure 5d1−d3 demonstrates the related DOS of the Ru-MoS_2 monolayer adsorbing three gas mixtures, from which the changes in the electronic properties of the Ru-MoS_2 monolayer upon adsorption of the gas mixtures can be seen. As can be seen from Figure 5d1, the adsorption performance of the Ru-MoS_2 monolayer toward the three gas mixtures results in a great enhancement of the electronic density of states of the Ru-MoS_2 monolayer, while the general profile does not change, indicating that the effect of the gas mixtures on the Ru-MoS_2 monolayer is synergistic and isotropic and that it does not change the properties of the Ru-MoS_2 monolayer. Figure 5d2 shows the partial DOS of the Ru atom and C atom that interact most with the Ru atom. The comparison of Figure 5a2−c2 reveals that the Fermi energy levels of the Ru atom are greatly enhanced by adsorption of mixed gases, which is due to the synergistic effect of the three gases on the charge transfer of the Ru-MoS_2 monolayer, and the result is in perfect agreement with Figure 5d1 and the EDD of mixed gas adsorption.

3.4. Band Structure (BS) Analysis. The electrical conductivity of sensing materials through band structure calculations can be predicted. Thus, the altered Ru-MoS_2 monolayer band gap following gas adsorption illustrates the change in its electrical conductivity in the presence of a specific gas. Increased conductivity is correlated with a narrower band gap and reduced conductivity with a broadened band gap. The band structures of the isolated Ru-MoS_2 monolayer, each VOC, and the mixed gas adsorption system are shown in Figure 6. It can be seen that the band gap of the Ru-MoS_2 monolayer (0.082 eV) is much smaller than that of the pristine MoS_2 monolayer of 1.9 eV, indicating the substantially enhanced conductivity of the Ru-MoS_2 monolayer. The band gaps of C_3H_4O, C_3H_6O, C_5H_8, and mixed gas adsorption

https://doi.org/10.1021/acsomega.3c09191
ACS Omega 2024, 9, 13951−13959

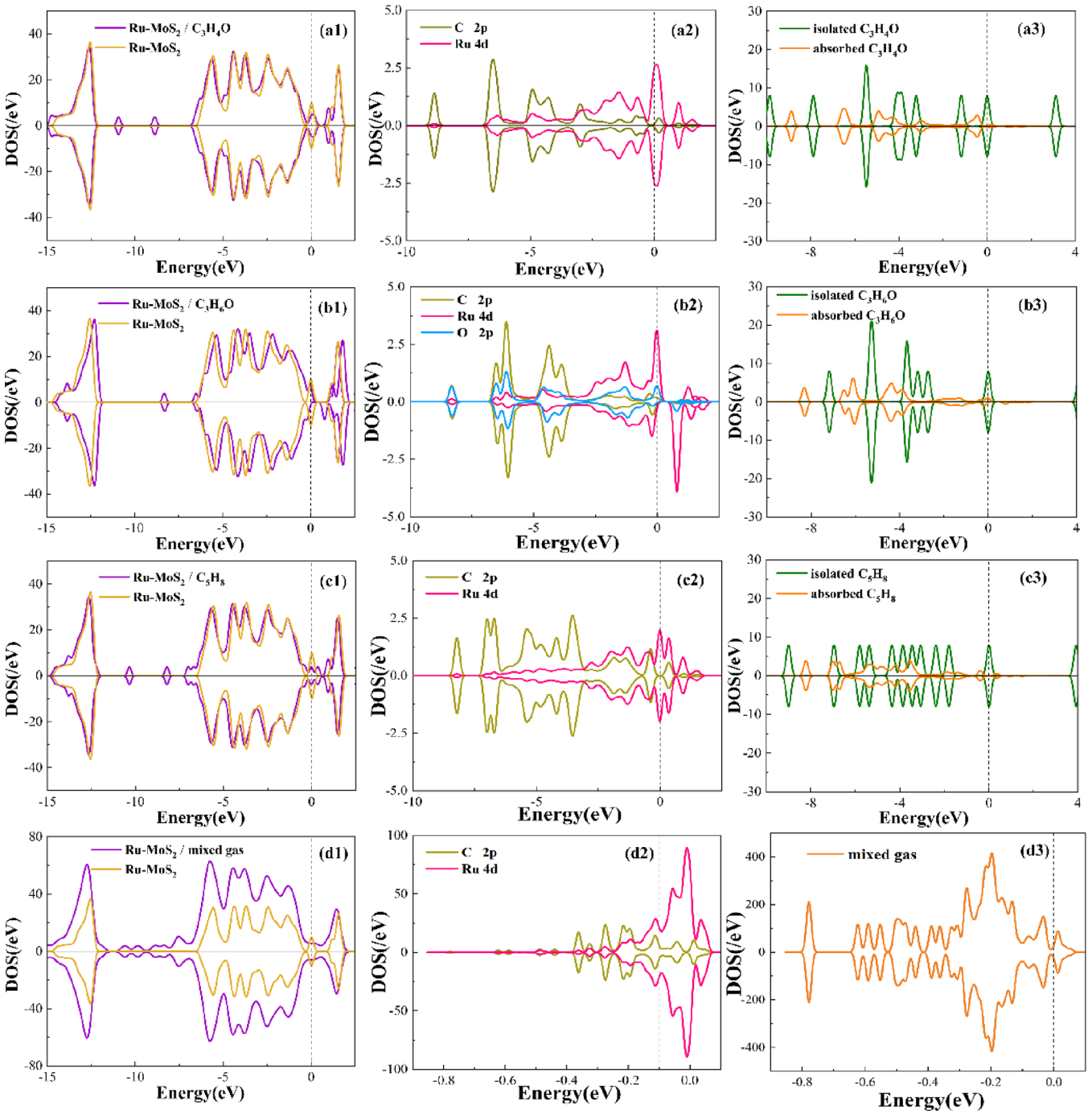

Figure 5. DOS of (a1−a3) the C_3H_4O system, (b1−b3) C_3H_6O system, (c1−c3) C_5H_8 system, and (d1−d3) mixed gas adsorption system. The dashed line is the Fermi level.

systems are 0.184, 0.767, 0.348, and 0.314 eV, respectively, which increased to varying degrees compared to the band gaps before adsorption, making it harder for electrons to be excited and decreasing the overall conductivity. The band gap change of the mixed gas adsorption system is the result of the combined action of three VOCs. It is discovered that, in contrast to the order of E_{ad} (C_3H_6O < C_5H_8 < C_3H_4O), the rising order of the band gaps in the three systems is C_3H_6O > C_5H_8 > C_3H_4O. The stronger Ru−C bond than the weaker Ru−O bond is thought to be the potential cause of the greater E_{ad}. Furthermore, the C_5H_8 molecule is larger in size than the C_3H_4O molecule, resulting in a lower E_{ad} due to the fact that it is easier to be trapped to produce the Ru−C bond. Thus, the band gap shift in the gas adsorption system might not be directly proportional to the E_{ad} value.

The conductivity (σ) and sensitivity (S) are crucial factors for resistive gas sensors. The characteristic gas species to be detected is assessed using the sensed response, which is based on the resistance changes before and after gas adsorption. The formulas for the calculation are given below:[33,34]

$$\sigma = A \cdot e^{(-B_g/2kT)} \tag{2}$$

$$S = (\sigma^{-1}_{gas} - \sigma^{-1}_{pure})/\sigma^{-1}_{pure} = (\sigma_{pure} - \sigma_{gas})/\sigma_{gas} \tag{3}$$

https://doi.org/10.1021/acsomega.3c09191
ACS Omega 2024, 9, 13951−13959

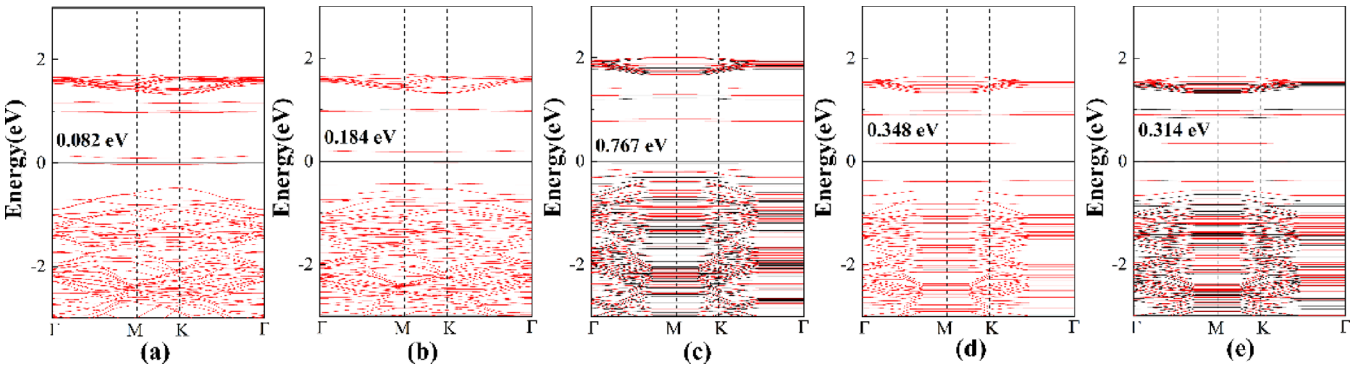

Figure 6. Band structure of the isolated Ru-MoS_2 monolayer and adsorbed systems. (a) Pristine Ru-MoS_2 monolayer; (b) C_3H_4O system; (c) C_3H_6O system; (d) C_5H_8 system; (e) mixed gas system. The black values are the band gap of a related system.

where A, B_g, k, and T mean the certain constant, band gap, Boltzmann constant, and working temperature in formula 2, respectively. In formula 3, σ_{gas} and σ_{pure} represent the conductivity of the adsorption system and isolated Ru-MoS_2 monolayer, respectively. The sensitivity reflects the reaction degree of the resistive gas sensor to the measured gas by monitoring the change of resistance. The computed findings demonstrate the sensitivity of the Ru-MoS_2 monolayer for C_3H_4O, C_3H_6O, and C_5H_8 to be 1.09, 140.50, and 5.90 at room temperature (298 K), respectively, which shows that the gas sensing material is quite sensitive to the target gas, and the resistance change can be intuitively generated. These results demonstrate the superior gas-sensitive performance for these gases, particularly the comparatively high sensitivity for C_3H_6O. The significant changes in the conductivity of Ru-MoS_2 monolayers caused by gas adsorption are sufficient for their detection. Therefore, the Ru-MoS_2 monolayer will be quite promising for clinical lung cancer diagnostic applications as a novel resistive sensing material for detecting the exhaled characteristic gases of lung cancer, C_3H_4O, C_3H_6O, and C_5H_8.

3.5. Work Function (WF) Analysis. To further understand the adsorption behavior of the doped system for each VOC gas, the work function (Φ) of each adsorption system is calculated, as shown in Figure 7. The variation of the work function is an important parameter for studying the gas-sensitive properties of materials, as is the variation of the electronic structure. The work function is the minimum energy required to move an electron from the Fermi energy level to infinity, and the variation of the work function directly affects the conductivity of the material, which can be calculated as[35,36]

$$\Phi = V_{vac} - E_f \quad (4)$$

where Φ is the work function, V_{vac} is the electrostatic potential at the vacuum level, and E_f is the Fermi energy. The work function for the Ru-MoS_2 monolayer is calculated to be 5.252 eV, and the work function after adsorption of C_3H_4O, C_3H_6O, and C_5H_8 has varying increases to 5.524, 5.415, and 5.306 eV, respectively. Due to the transfer of charge, the Fermi energy level and work function change accordingly, and when the electrons are drawn out, the Fermi energy level of the system drops while the work function rises. The Q_T values of C_3H_4O, C_3H_6O, and C_5H_8 adsorption systems are −0.225 e, −0.133 e, and −0.120 e, respectively, which are consistent with the change of the work function.

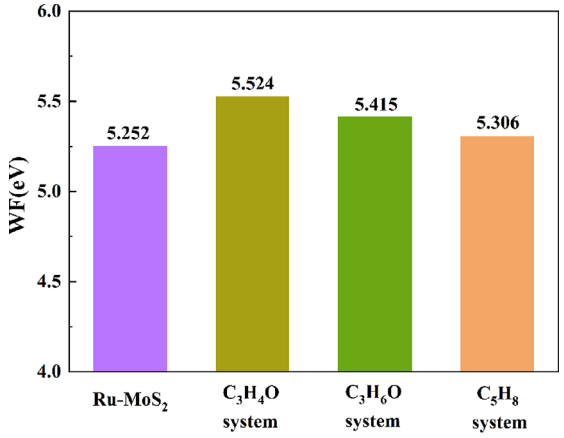

Figure 7. Work function of the isolated Ru-MoS_2 monolayer and various adsorption systems.

In view of the fact that the gas sensor will be exposed to the atmosphere in the practical application, the influence of O_2 and N_2 on the adsorption of VOCs by the Ru-MoS_2 monolayer is considered in this work. The gas mixture adsorption configurations of VOCs and O_2 (or N_2) molecule are carried out and BSs are examined to understand their impacts in this study, as shown in Figure 8. It can be seen that the presence of an O_2 molecule considerably weakens the band gap of the adsorption system, whereas the presence of N_2 molecules has almost no effect on the band gap of the Ru-MoS_2 monolayer for the gas mixture adsorption systems of C_3H_4O/N_2 and C_5H_8/N_2, with the exception of C_3H_6O/N_2. It is also worth noting that in the three adsorption systems containing O_2, the band gap is almost zero and the systems exhibit metallic properties. The presence of the O_2 molecule will promote strong n-type doping in the mixed adsorption system of O_2 and VOCs, and the electrons will be released back into the conduction band of the Ru-MoS_2 monolayer, leading to a reduction in the thickness of the electron depletion region and an increase in the overall conductivity of the Ru-MoS_2 monolayer, which will have a contributing effect on the sensing response for gas detection. Based on the above analysis, it can be seen that atmospheric O_2 and N_2 will not hinder the adsorption of the three VOCs on the Ru-MoS_2 monolayer. Therefore, it can be hypothesized that the Ru-MoS_2 monolayer is expected to be used as a resistive gas sensor for the detection of exhaled breath for early lung cancer screening.

https://doi.org/10.1021/acsomega.3c09191
ACS Omega 2024, 9, 13951−13959

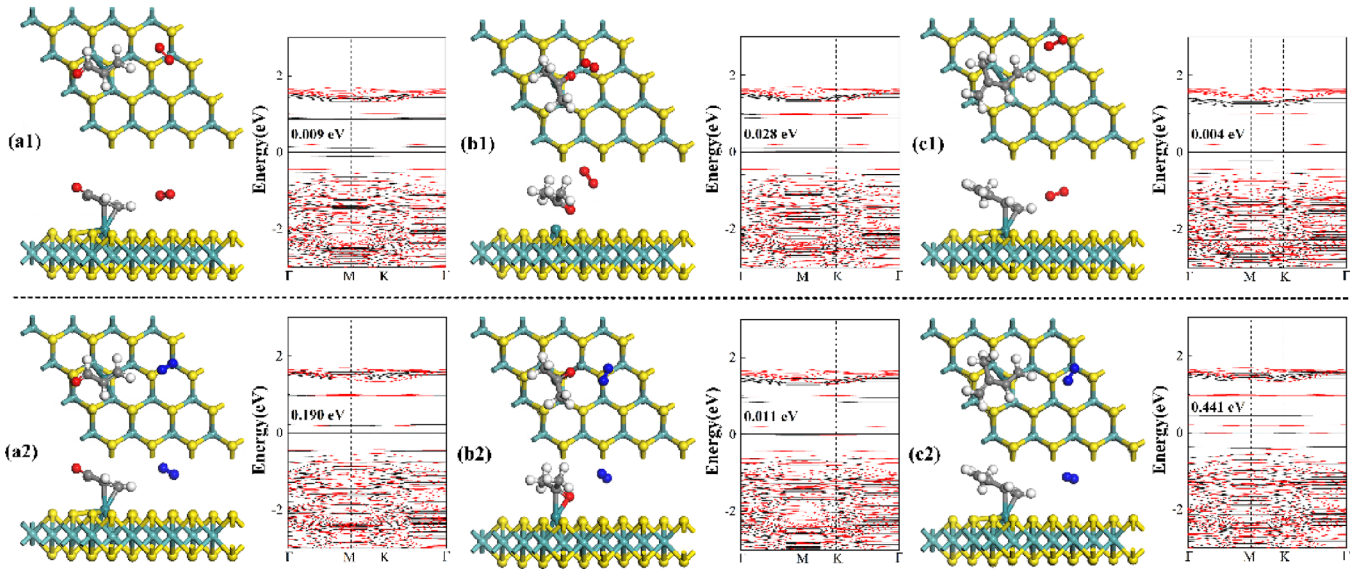

Figure 8. Gas mixture adsorption configuration and BS. (a1) C_3H_4O/O_2 system; (a2) C_3H_4O/N_2 system; (b1) C_3H_6O/O_2 system; (b2) C_3H_6O/N_2 system; (c1) C_5H_8/O_2 system; (c2) C_5H_8/N_2 system.

4. CONCLUSIONS

Based on first principles, the gas sensing properties of the transition metal Ru-doped MoS_2 monolayer for C_3H_4O, C_3H_6O and C_5H_8 gases have been systematically investigated to explore their potential as a resistive gas sensor for the early diagnosis of lung cancer. In this study, the adsorption energy, charge transfer, electronic behavior, band structure, and work function of the adsorption system are calculated. In addition, the sensitivity of the Ru-MoS_2 monolayer to each gas is investigated to fully understand its application characteristic properties as a gas sensor. The following are the primary conclusions:

(1) A Ru dopant replacement of a S atom forms a stabilized Ru-MoS_2 monolayer with a binding energy of −4.78 eV, and the thermostability and chemical stability are further confirmed. In addition, the doping of Ru could improve the adsorption performance for the three VOCs as calculated.

(2) C_3H_4O, C_3H_6O, and C_5H_8 can be stably adsorbed on the Ru-MoS_2 surface with E_{ad} values of −3.42, −1.53, and −2.80 eV, respectively, all of which are chemisorption. EDD and DOS are used to further understand the adsorption behavior of gas molecules on Ru-MoS_2 monolayers.

(3) The band structure and work function analysis reveal the conductivity change and sensing mechanism of gas adsorption by Ru-MoS_2 monolayers, and the sensitivities for three gases at room temperature are obtained as 1.09, 140.50, and 5.90, respectively.

In this study, the strong potential of Ru-MoS_2 monolayers as novel 2D TMD gas sensing material for the detection of exhaled characteristic gases of lung cancer has been explored, which provides theoretical guidance for the application in practical lung cancer diagnosis. Nevertheless, the Ru-MoS_2 monolayer discussed in this work still has certain defects, such as weak selectivity for specific VOCs. Therefore, it is necessary to solve the problem of cross interference of mixed gases in the practical application of gas sensors in the later period, such as using neural network algorithms. On the other hand, continuing to explore sensing materials with high selectivity and high sensitivity for specific VOCs is also a challenge to be overcome in the future.

AUTHOR INFORMATION

Corresponding Author

Qianqian Wan − *Department of Rheumatology, Zhongnan Hospital of Wuhan University, Wuhan 430072, China;* orcid.org/0000-0002-4899-963X; Email: wanqq@whu.edu.cn

Author

Xiaoqi Chen − *Department of Rheumatology, Zhongnan Hospital of Wuhan University, Wuhan 430072, China*

Complete contact information is available at: https://pubs.acs.org/10.1021/acsomega.3c09191

Funding

This research received no external funding.

Notes

The authors declare no competing financial interest.

REFERENCES

(1) Jia, Z.; Patra, A.; Kutty, V.; Venkatesan, T. Critical Review of Volatile Organic Compound Analysis in Breath and In Vitro Cell Culture for Detection of Lung Cancer. *Metabolites* **2019**, *9* (3), 52.

(2) Koureas, M.; Kirgou, P.; Amoutzias, G.; Hadjichristodoulou, C.; Gourgoulianis, K.; Tsakalof, A. Target Analysis of Volatile Organic Compounds in Exhaled Breath for Lung Cancer Discrimination from Other Pulmonary Diseases and Healthy Persons. *Metabolites* **2020**, *10* (8), 317.

(3) Chang, J.-E.; Lee, D.-S.; Ban, S.-W.; Oh, J.; Jung, M. Y.; Kim, S.-H.; Park, S.; Persaud, K.; Jheon, S. Analysis of volatile organic compounds in exhaled breath for lung cancer diagnosis using a sensor system. *Sens. Actuators, B* **2018**, *255*, 800−807.

(4) Hakim, M.; Broza, Y. Y.; Barash, O.; Peled, N.; Phillips, M.; Amann, A.; Haick, H. Volatile Organic Compounds of Lung Cancer and Possible Biochemical Pathways. *Chem. Rev.* **2012**, *112* (11), 5949−5966.

(5) Jia, Z.; Zhang, H.; Ong, C. N.; Patra, A.; Lu, Y.; Lim, C. T.; Venkatesan, T. Detection of Lung Cancer: Concomitant Volatile Organic Compounds and Metabolomic Profiling of Six Cancer Cell Lines of Different Histological Origins. *ACS Omega* **2018**, *3* (5), 5131−5140.

(6) Chen, X.; Muhammad, K. G.; Madeeha, C.; Fu, W.; Xu, L.; Hu, Y.; Liu, J.; Ying, K.; Chen, L.; Yurievna, G. O. Calculated indices of volatile organic compounds (VOCs) in exhalation for lung cancer screening and early detection. *Lung Cancer* **2021**, *154*, 197−205.
(7) Sam, D.; Cheung, W. A population-level comparison of cancer-related and non-cancer-related health care costs using publicly available provincial administrative data. *Current Oncology* **2019**, *26* (2), 94−97.
(8) Gaude, E.; Nakhleh, M. K.; Patassini, S.; Boschmans, J.; Allsworth, M.; Boyle, B.; Van Der Schee, M. P. Targeted breath analysis: exogenous volatile organic compounds (EVOC) as metabolic pathway-specific probes. *Journal of Breath Research* **2019**, *13* (3), No. 032001.
(9) Siegel, R. L.; Miller, K. D.; Jemal, A. CA: a cancer journal for clinicians. *Cancer statistics, 2019* **2019**, *69* (1), 7−34.
(10) Wang, P.; Huang, Q.; Meng, S.; Mu, T.; Liu, Z.; He, M.; Li, Q.; Zhao, S.; Wang, S.; Qiu, M. Identification of lung cancer breath biomarkers based on perioperative breathomics testing: A prospective observational study. *EClinicalMedicine* **2022**, *47*, No. 101384.
(11) Pisapia, P.; Pepe, F.; Baggi, A.; Barberis, M.; Galvano, A.; Gristina, V.; Mastrilli, F.; Novello, S.; Pagni, F.; Pasini, S.; Perrone, G.; Righi, D.; Russo, A.; Troncone, G.; Malapelle, U. Next generation diagnostic algorithm in non-small cell lung cancer predictive molecular pathology: The KWAY Italian multicenter cost evaluation study. *Crit. Rev. Oncol./Hematol.* **2022**, *169*, No. 103525.
(12) Gordon, S.; Szidon, J.; Krotoszynski, B.; Gibbons, R.; O'neill, H. Volatile organic compounds in exhaled air from patients with lung cancer. *Clinical chemistry* **1985**, *31* (8), 1278−1282.
(13) Barash, O.; Tisch, U.; Haick, H. Volatile organic compounds and the potential for a lung cancer breath test. *Lung Cancer Management* **2013**, *2* (6), 471−482.
(14) Sun, C.; Wang, L.; Zhao, W.; Xie, L.; Wang, J.; Li, J.; Li, B.; Liu, S.; Zhuang, Z.; Zhao, Q. Atomic-Level Design of Active Site on Two-Dimensional MoS_2 toward Efficient Hydrogen Evolution: Experiment, Theory, and Artificial Intelligence Modelling. *Adv. Funct. Mater.* **2022**, *32* (38), No. 2206163.
(15) Xu, J.; Shao, G.; Tang, X.; Lv, F.; Xiang, H.; Jing, C.; Liu, S.; Dai, S.; Li, Y.; Luo, J.; Zhou, Z. Frenkel-defected monolayer MoS_2 catalysts for efficient hydrogen evolution. *Nat. Commun.* **2022**, *13* (1), 2193.
(16) Wang, J.; Zhang, X.; Liu, L.; Wang, Z. Adsorption of SF_6 Decomposition Products by the S Vacancy Structure and Edge Structure of SnS_2: A Density Functional Theory Study. *ACS Omega* **2021**, *6* (42), 28131−28139.
(17) Zhao, G.; Li, M. Ni-doped MoS2 biosensor: a promising candidate for early diagnosis of lung cancer by exhaled breathe analysis. *Appl. Phys. A* **2018**, *124*, 1−9.
(18) Li, B.; Zhou, Q.; Peng, R.; Liao, Y.; Zeng, W. Adsorption of SF_6 decomposition gases (H_2S, SO_2, SOF_2 and SO_2F_2) on Sc-doped MoS_2 surface: A DFT study. *Appl. Surf. Sci.* **2021**, *549*, No. 149271.
(19) Gui, Y.; Shi, J.; Yang, P.; Li, T.; Tang, C.; Xu, L. Platinum modified MoS_2 monolayer for adsorption and gas sensing of SF_6 decomposition products: A DFT study. *High Voltage* **2020**, *5* (4), 454−462.
(20) Cui, H.; Zhang, X.; Zhang, G.; Tang, J. Pd-doped MoS_2 monolayer: a promising candidate for DGA in transformer oil based on DFT method. *Appl. Surf. Sci.* **2019**, *470*, 1035−1042.
(21) Chen, D.; Zhang, X.; Tang, J.; Cui, H.; Li, Y. Noble metal (Pt or Au)-doped monolayer MoS_2 as a promising adsorbent and gas-sensing material to SO_2, SOF_2 and SO_2F_2: a DFT study. *Appl. Phys. A* **2018**, *124* (2), 194.
(22) Zhang, G.; Wang, Z.; Zhang, X. Theoretical screening into Ru-doped MoS_2 monolayer as a promising gas sensor upon SO_2 and SOF_2 in SF_6 insulation devices. *Mol. Phys.* **2021**, *120*, No. e2018517.
(23) Wang, Z.; Zhao, J.; Cai, Q.; Li, F. Computational screening for high-activity MoS_2 monolayer-based catalysts for the oxygen reduction reaction via substitutional doping with transition metal. *Journal of Materials Chemistry A* **2017**, *5* (20), 9842−9851.
(24) Fan, Y.; Zhang, J.; Qiu, Y.; Zhu, J.; Zhang, Y.; Hu, G. A DFT study of transition metal (Fe, Co, Ni, Cu, Ag, Au, Rh, Pd, Pt and Ir)-embedded monolayer MoS_2 for gas adsorption. *Comput. Mater. Sci.* **2017**, *138*, 255−266.
(25) Liu, T.; Cui, Z.; Li, X.; et al. Al-doped $MoSe_2$ monolayer as a promising biosensor for exhaled breath analysis: a DFT study[J]. *ACS omega* **2021**, *6* (1), 988−995.
(26) Liu, H.; Luo, X. Au-and Pd-Doped SnS_2 Monolayers for Lung Cancer Biomarkers (C_3H_6O, C_6H_6, and C_5H_8) Detection: A Density Functional Theory Investigation. *ACS Omega* **2023**, 7658.
(27) Wu, J.; Li, Z.; Luo, A.; et al. A DFT Study of Volatile Organic Compounds Detection on Pristine and Pt-Decorated SnS Monolayers[J]. *Sensors* **2023**, *23* (17), 7319.
(28) Peng, R.; Zeng, W.; Zhou, Q. Adsorption and gas sensing of dissolved gases in transformer oil onto Ru_3-modified SnS_2: A DFT study. *Appl. Surf. Sci.* **2023**, *615*, No. 156445.
(29) Wu, Y.; Wang, X.; Duan, Y.; Peng, M. Revealing boron adsorption on the α-Ti (0001) surface by first-principles calculations. *Philos. Mag.* **2022**, *102* (18), 1873−1890.
(30) Wu, Y.; Ding, D.; Wang, Y.; Zhou, C.; Lu, H.; Zhang, X. Defect recognition and condition assessment of epoxy insulators in gas insulated switchgear based on multi-information fusion. *Measurement* **2022**, *190*, No. 110701.
(31) Li, Z.; Liao, Y.; Liu, Y.; Zeng, W.; Zhou, Q. Room temperature detection of nitrogen dioxide gas sensor based on Pt-modified $MoSe_2$ nanoflowers: Experimental and theoretical analysis. *Appl. Surf. Sci.* **2023**, *610*, No. 155527.
(32) Wan, Q.; Chen, X.; Xiao, S. Ru-Doped $PtTe_2$ Monolayer as a Promising Exhaled Breath Sensor for Early Diagnosis of Lung Cancer: A First-Principles Study. *Chemosensors* **2022**, *10* (10), 428.
(33) Li, Z.; Jia, L.; Chen, J.; Cui, X.; Zeng, W.; Zhou, Q. Ag-modified hexagonal GaN monolayer as an innovative gas detector toward SF_6 decomposed species: Insights from the first-principles computations. *Appl. Surf. Sci.* **2022**, *589*, No. 153000.
(34) Hou, W.; Liu, Y.; Zeng, W.; Zhou, Q. Theoretical screening into Ag-Embedded HfS_2 monolayers as gas sensor for detecting SF_6 decomposition gases. *Journal of Materials Research and Technology* **2022**, *18*, 1991−2000.
(35) Lu, Z.; Zhai, Y.; Liang, Q.; Wu, W. Promoting sensitivity and selectivity of NO_2 gas sensor based on metal (Pt, Re, Ta)-doped monolayer WSe_2: A DFT study. *Chem. Phys. Lett.* **2020**, *755*, No. 137737.
(36) Wang, Z.; Zhang, X.; Yuan, J.; Tan, S. Ni-doped $HfSe_2$ monolayer as a gas scavenger toward SO_2 and SOF_2: a DFT study. *Mol. Phys.* **2023**, No. e2202282.

https://doi.org/10.1021/acsomega.3c09191
ACS Omega 2024, 9, 13951−13959